A Split-Operator, Finite-Difference Solution for Axisymmetric Laminar-Jet Diffusion Flames

R. J. Kee* and J. A. Miller†
Sandia Laboratories, Livermore, Calif.

A split-operator numerical method is developed to solve the steady laminar diffusion flame problem. Splitting the chemical kinetic terms from the fluid-mechanical terms ameliorates some of the difficulties associated with the disparate time scales and stiffness in the set of equations which describes highly exothermic diffusion flames. Implicit differencing methods enhance the numerical stability of both operators. Special care is taken to maintain the accuracy of the solution, and the coordinate system is varied continuously to follow the flame shape. The present method allows a detailed study of the complex interaction between the fluid mechanics and the finite-rate chemical kinetics in a flame.

Nomenclature

C_p = constant-pressure heat capacity of the gas mixture
C_{pk} = constant-pressure heat capacity of the kth species
D_k = trace diffusion coefficient of kth species
g = acceleration due to gravity
h_k = enthalpy of species k per unit mass
J = number of radial nodes
K = number of species
p = pressure
r = radial dimension
R = universal gas constant, ergs/mole-K
S = source term in general transport equation
T = temperature
u = axial velocity
v = radial velocity
V = transformed radial velocity
$\dot{\omega}_k$ = formation rate of kth species by chemical reaction
W_k = molecular weight of kth species
x = axial dimension
Y_k = mass fraction of kth species
α = coordinate spread angle
ξ = transformed axial dimension
ξ_0 = origin of coordinate system referenced to nozzle exit
ϵ = transport coefficient in general transport equation
λ = conductivity
η = transformed radial coordinate
ρ = mass density of the gas mixture
μ = viscosity
X_k = chemical symbol for kth species

Subscripts

i = axial node index
j = radial node index
k = species index
n = reaction index
e = edge condition

Introduction

COMBUSTION processes are characterized by the existence of multiple, vastly differing time and length scales, and thus their computational description suffers from a number of associated difficulties. Numerical methods have not been developed to handle adequately these highly exothermic, chemically reacting flows. Without accurate prediction schemes, the dual goal of producing more efficient combustors and at the same time reducing their pollutant output is exceedingly difficult. The problem of the laminar-jet diffusion flame is typical of many combustion problems, and, consequently, it embodies common computational difficulties. For this reason, and because uncertainties in the reaction mechanisms and transport properties are minimized, we have chosen to develop a numerical model for the hydrogen-air diffusion flame.

The basic configuration is a fuel jet that is issuing vertically into ambient, still air, and the flame has been ignited long enough for a steady flow to develop. A flame zone can be defined by a thin, high-temperature region, which, beginning at the nozzle tip, bows radially outward before eventually converging at the jet centerline. Flame length, typically thought of as the distance from the nozzle to the point of peak centerline temperature, increases as the inlet fuel flow rate increases. Although the peak temperatures converge toward the centerline, the complete region of elevated temperatures spreads monotonically.

The convective and diffusive processes that describe the flame are characterized by one time scale, whereas the chemical kinetics processes in the highly active reaction zone are characterized by a much smaller time scale. Moreover, the chemical time scale itself is broken up into widely varying time scales. For example, the creation and destruction rates for reaction intermediates, particularly free radicals, are much faster than the rates for the overall conversion of reactants to products.

Since the flames studied here are characterized by axial convective fluxes that are much larger than the diffusive fluxes, it is appropriate to employ the boundary-layer assumptions in the governing equations. However, a full finite-rate, chemical kinetics mechanism is incorporated. An operator-splitting method is used to deal effectively with the disparate chemical and fluid-mechanics scales, and use of the Hindmarsh-Gear[1] algorithm serves to resolve the difficulties of stiffness and disparate time scales within the chemical-rate equations.

The solutions are computed on a finite-difference grid network. Through an analytic variable transformation, this grid system is altered continuously to follow the flame shape and maintain maximum radial resolution in the finite-difference equations. The axial step size is adjusted automatically to insure that the difference equations have converged to within a prespecified error tolerance.

In the present paper, we develop briefly the physical and chemical model. However, we describe in detail the numerical

Received June 15, 1977; presented as Paper 77-639 at the AIAA 3rd Computational Fluid Dynamics Conference, Albuquerque, N. Mex., June 27-28, 1977; revision received Sept. 26, 1977.

Index category: Computational Methods.

*Staff Member.
†Staff Member. Member AIAA.

method that we have used and discuss its application. In a companion paper,[2] we present the result of our calculations, concentrating on the chemical mechanism and the roles of the reaction intermediates.

Physical and Chemical Model

Governing Equations

Instead of the Navier-Stokes equations, we use the boundary-layer equations, together with an assumption of uniform pressure; and, as a result, we obtain a set of parabolic, rather than elliptic, equations. Because the pressures are low and the temperatures are high, the assumption of a thermally perfect gas is valid.

By transforming from cylindrical coordinates to similarity-like variables, some computational advantages can be achieved. The new idependent variables are

$$\eta(r,x)=r/x \tag{1}$$

$$\xi(x)=x \tag{2}$$

This transformation removes the locally linear boundary-layer growth which results from a spreading of the jet in order to conserve mass, momentum, and energy. One new dependent variable also is introduced and is given by

$$V=\eta\rho v-\eta^2\rho u \tag{3}$$

To obtain a definition of the coordinate system, we specify an origin ξ_0 and a spread angle α. The η coordinate varies from zero at the centerline to $\eta_e=\tan\alpha$ at the outer edge. Absolute values of x have no meaning in the physical equations; however, because the transformation is singular, ξ itself does appear in the governing equations, and it must be referenced to the origin of the coordinate system ξ_0. After each downstream step in the numerical procedure, we can adjust the values of ξ_0 and α to account for the local jet growth. The transformed governing equations are stated below:

Continuity

$$\xi\frac{\partial\rho u}{\partial\xi}+\frac{1}{\eta}\frac{\partial V}{\partial\eta}+2\rho u=0 \tag{4}$$

Axial Momentum

$$\rho u\xi\frac{\partial u}{\partial\xi}+\frac{V}{\eta}\frac{\partial u}{\partial\eta}=\frac{1}{\xi\eta}\frac{\partial}{\partial\eta}\left(\mu\eta\frac{\partial u}{\partial\eta}\right)+\xi(\rho_e-\rho)g \tag{5}$$

Thermal Energy

$$\rho u\xi\frac{\partial T}{\partial\xi}+\frac{V}{\eta}\frac{\partial T}{\partial\eta}=\frac{1}{C_p\xi\eta}\frac{\partial}{\partial\eta}\left(\lambda\eta\frac{\partial T}{\partial\eta}\right)+\frac{1}{C_p\xi}\times\sum_{k=1}^{K}\left(C_{p_k}\rho D_k\frac{\partial Y_k}{\partial\eta}\right)\frac{\partial T}{\partial\eta}-\frac{\xi}{C_p}\sum_{k=1}^{K}\dot{\omega}_k h_k W_k \tag{6}$$

Species

$$\rho u\xi\frac{\partial Y_k}{\partial\xi}+\frac{V}{\eta}\frac{\partial Y_k}{\partial\eta}=\frac{1}{\xi\eta}\frac{\partial}{\partial\eta}\left(\rho D_k\frac{\partial Y_k}{\partial\eta}\right)+\xi\dot{\omega}_k W_k \tag{7}$$

Equation of State

$$\rho=P\Big/\left(\sum_{k=1}^{K}\frac{Y_k R}{W_k}T\right) \tag{8}$$

Implicit in these equations are a number of assumptions. The effects of both thermal and pressure diffusion and viscous dissipation have been neglected. The diffusion coefficient D_k is a trace diffusion coefficient of the kth species in N_2. Justification for this formulation comes from recognizing that the principal constituent in the reaction zone is N_2 and that, moreover, the actual bimolecular diffusion coefficients do not vary greatly for the different species. A consequence of the trace diffusion coefficient approximation is that conservation of mass is not guaranteed. Therefore, only $K-1$ species equations should be solved, and the Kth species should be specified to satisfy

$$\sum_{k=1}^{K}Y_k=1$$

We choose not to solve a species conservation equation for N_2. Equations (4-8), together with the assumption of uniform pressure, form a set of $K+4$ equations for the dependent variables u, V, T, ρ, and Y_k.

Recognizing the common form of the transport equations and writing a general equation will facilitate further derivations. That equation is stated as

$$\rho u\xi\frac{\partial f}{\partial\xi}+\left(\frac{V}{\eta}+B\right)\frac{\partial f}{\partial\eta}=\frac{1}{a\xi\eta}\frac{\partial}{\partial\eta}\left(\epsilon\eta\frac{\partial f}{\partial\eta}\right)+\xi d+\xi S \tag{9}$$

The variable f represents either u, T, or Y_k, whereas d comes from the buoyancy term in the momentum equation, and S is the chemical source contribution in both the energy and species equations. The term B represents the energy transport caused by species diffusion velocities.

Rather than solve the continuity equation as it stands in Eq. (4), we find it advantageous to eliminate the ξ derivatives in the first term by substituting the transport equations. This elimination first requires that we differentiate the equation of state to procure an expression for $\partial\rho/\partial\xi$ in terms of $\partial T/\partial\xi$ and $\partial Y_k/\partial\xi$:

$$\frac{\partial\rho}{\partial\xi}=-\frac{p}{R}\left\{\left(T^2\sum_{k=1}^{K}\frac{Y_k}{W_k}\right)^{-1}\frac{\partial T}{\partial\xi}+\left[T\left(\sum_{k=1}^{K}\frac{Y_k}{W_k}\right)^2\right]^{-1}\sum_{k=1}^{K}\frac{1}{W_k}\frac{\partial Y_k}{\partial\xi}\right\} \tag{10}$$

The revised continuity equation is written as

$$\frac{V}{u}\frac{\partial u}{\partial\eta}-\frac{V}{T}\frac{\partial T}{\partial\eta}-\frac{\rho RTV}{p}\sum_{k=1}^{K}\left(\frac{1}{W_k}\frac{\partial Y_k}{\partial\eta}\right)-\frac{\partial V}{\partial\eta}=\frac{1}{\xi u}\frac{\partial}{\partial\eta}\left(\mu\eta\frac{\partial u}{\partial\eta}\right)-\frac{u}{C_pT\xi u}\frac{\partial}{\partial\eta}\left(\lambda\eta\frac{\partial T}{\partial\eta}\right)+\frac{\xi\eta}{C_pT}\sum_{k=1}^{K}\dot{\omega}_k h_k W_k-\frac{\rho RT}{P\xi}\sum_{k=1}^{K}\left[\frac{1}{W_k}\frac{\partial}{\partial\eta}\left(\rho D_k\eta\frac{\partial Y_k}{\partial\eta}\right)\right]-\frac{\rho RT\eta\xi}{P}\sum_{k=1}^{K}\dot{\omega}_k+2\eta\rho u-\frac{\eta}{C_pT\xi}\sum_{k=1}^{K}\left(C_{p_k}\rho D_k\frac{\partial Y_k}{\partial\eta}\right)\frac{\partial T}{\partial\eta}+\frac{\xi\eta}{u}(\rho_e-\rho)g \tag{11}$$

Such a formulation, first suggested by Krause,[3] allows us to solve for V from T, u, and Y_k at any axial location by solving a first-order initial-value problem.

Thermodynamic and Transport Properties

All transport properties for individual species have been calculated from the appropriate Enskog-Chapman expressions using the Lennard-Jones parameters given by Svehla.[4] Correlations of these properties as a function of temperature have been given by Pohl[5] and are used in the calculations presented here. The viscosity and conductivity of the gas mixture are obtained from the single-component

transport properties using Wilke's semiempirical formulas. (See Ref. 2 for more details.)

Thermodynamic properties (heat capacities, entropies, and enthalpies) are computed from the JANNAF data used in the NASA Complex Chemical Equilibrium Code.[6] Equilibrium constants in terms of partial pressures are obtained from the relation

$$K_{p_n} = \exp(-\Delta H_n/RT + \Delta S_n/R) \tag{12}$$

where ΔH and ΔS refer to the change that occurs in the standard state enthalpies and entropies in passing from reactants to products by the nth elementary chemical reaction. The corresponding equilibrium constant in terms of concentrations is given by Eq. (3):

$$K_{c_n} = K_{p_n}\left(\frac{1.01325\times 10^6}{RT}\right)^{\mathcal{Q}} \tag{13}$$

where

$$\mathcal{Q} = \sum_{k=1}^{K} (\nu''_{nk} - \nu'_{nk})$$

and ν''_{nk} and ν'_{nk} are stoichiometric coefficients in the nth reaction.

Chemical Kinetic Formulation

The elementary chemical reactions are expressed as

$$\sum_{k=1}^{K} \nu'_{nk} X_k \rightleftharpoons \sum_{k=1}^{K} \nu''_{nk} X_k \tag{14}$$

The rate-of-progress variable for the nth reaction $\dot{\delta}_n$ is defined as the forward rate minus the reverse rate, as stated in Eq. (15):

$$\dot{\delta}_n = k_{f_n} \prod_{k=1}^{K} [X_k]^{\nu'_{nk}} - k_{r_n} \prod_{k=1}^{K} [X_k]^{\nu''_{nk}} \tag{15}$$

The species production terms in the conservation equations are found from

$$\dot{\omega}_k = \sum_{n=1}^{N} \nu_{nk} \dot{\delta}_n \tag{16}$$

where $\nu_{nk} = \nu''_{nk} - \nu'_{nk}$. The reverse rates are given in terms of the forward rates and the equilibrium constants as

$$k_{r_n} = k_{f_n}/K_{c_n} \tag{17}$$

The calculations that we give in this paper to illustrate our method involve the oxidation of molecular hydrogen by air. The specific reaction mechanism involves 10 species (H_2, O_2, N_2, H, O, N, OH, HO_2, H_2O, NO) and is listed in Table 1. Also listed are the forward rate constants, which have the common form

$$k_{f_n} = A_n T^{\beta_n} \exp(-E_n/RT) \tag{18}$$

These rate constants have been compiled from numerous sources in the current literature; the specific references are given in Ref. 2.

Initial and Boundary Conditions

The governing set of partial differential equations is parabolic in nature; thus boundary conditions are required at $\eta = 0$ and $\eta = \eta_e$, and initial conditions must be imposed at the burner exit plane. The centerline $\eta = 0$ is an axis of symmetry; therefore, conditions

$$\left(\frac{\partial u}{\partial \eta}\right)_0 = \left(\frac{\partial T}{\partial \eta}\right)_0 = \left(\frac{\partial Y_k}{\partial \eta}\right)_0 = (V)_0 = 0 \tag{19}$$

Table 1 Reaction mechanism for H_2-air combustion

Reaction	A_n	β_n	E_n, cal/mole
1) $H_2 + O_2 \rightleftharpoons 2OH$	1.7×10^{13}	0.0	47,780.0
2) $H_2 + OH \rightleftharpoons H_2O + H$	5.2×10^{13}	0.0	6,550.0
3) $H + O_2 \rightleftharpoons OH + O$	1.22×10^{17}	−0.907	16,620.0
4) $O + H_2 \rightleftharpoons OH + H$	1.8×10^{10}	1.0	8,826.0
5) $H + O_2 + M \rightleftharpoons HO_2 + M$	2.0×10^{15}	0.0	−870.0
6) $OH + HO_2 \rightleftharpoons H_2O + O_2$	1.2×10^{13}	0.0	0.0
7) $H + HO_2 \rightleftharpoons 2OH$	6.0×10^{13}	0.0	0.0
8) $O + HO_2 \rightleftharpoons O_2 + OH$	1.0×10^{13}	0.0	0.0
9) $OH + OH \rightleftharpoons O + H_2O$	1.7×10^{6}	2.03	−1,190.0
10) $H_2 + M \rightleftharpoons H + H + M$	2.23×10^{12}	0.5	92,600.0
$M = H_2O$	1.15×10^{13}		
11) $O_2 + M \rightleftharpoons O + O + M$	1.85×10^{11}	0.5	95,560.0
12) $H + OH + M \rightleftharpoons H_2O + M$	7.5×10^{23}	−2.6	0.0
$M = H_2O$	1.5×10^{25}		
13) $O + N_2 \rightleftharpoons NO + N$	1.4×10^{14}	0.0	75,800.0
14) $N + O_2 \rightleftharpoons NO + O$	6.4×10^{9}	1.0	6,280.0
15) $OH + N \rightleftharpoons NO + H$	4.0×10^{13}	0.0	0.0
16) $H + HO_2 \rightleftharpoons H_2 + O_2$	1.3×10^{13}	0.0	0.0

must be applied there. At the outer edge of the jet, all of the dependent variables must become equal to their ambient freestream values:

$$(u)_{\eta_e} = u_e, \quad (T)_{\eta_e} = T_e, \quad (Y_k)_{\eta_e} = Y_{k_e} \tag{20}$$

Since it is both inconvenient and inefficient to have $\eta_e \to \infty$ in a numerical calculation, it is necessary to insure by some alternative means that radial gradients vanish at the outer edge of the jet. Otherwise, the result would be a net loss of mass, momentum, and energy from the flame. This condition is satisfied by a continuous adjustment of the coordinate system to appropriate values of η_e. Such a specification is discussed more completely in the section describing the solution methods. Equation (11), which is used to solve for V, is first order in η; thus no boundary condition on V at $\eta = \eta_e$ is required. As a consequence of the calculation, the entrainment rate at the edge of the jet is determined.

Although the boundary conditions are straightforward, the formulation of the initial conditions requires some physical insight and judgment. At the exit plane of the burner nozzle, all of the dependent variables must be specified so that the correct flame structure develops as the solution proceeds downstream. The axial velocity profile is assumed to have the form of the similar solution for an incompressible isothermal circular jet.[7]

Physically, one expects that a narrow mixing zone must exist in the vicinity of the burner lip prior to ignition of the gases by radiation and axial heat conduction. Of course, the boundary-layer approximation does not allow for upstream energy transport. Thus it is necessary to specify as initial conditions that the fuel and air have been mixed over a narrow region near the lip and raised to a temperature high enough to allow rapid chemical reaction and energy release to occur where the fuel and oxygen have mixed to ignitable proportions. We assume the initial species distributions to be in the form of arc-cotangent functions. These are only smoothing functions and have no special physical significance. They are used only to avoid numerical difficulties with step function changes in the initial conditions.

The temperature profile at the burner exit is specified in the form of a gaussian function, which is centered at the nozzle lip. (This is also the stoichiometric point.) Its height is taken at about the observed flame temperature (~2100 K), and its width is adjusted so that the region of elevated temperature is confined to the mixing zone. There is considerable latitude available in specifying the initial temperature profile. It is necessary, however, that the temperatures be high enough and the gradients small enough to allow the chain branching reactions to occur; i.e., the reaction $H + O_2 - OH + O$ must

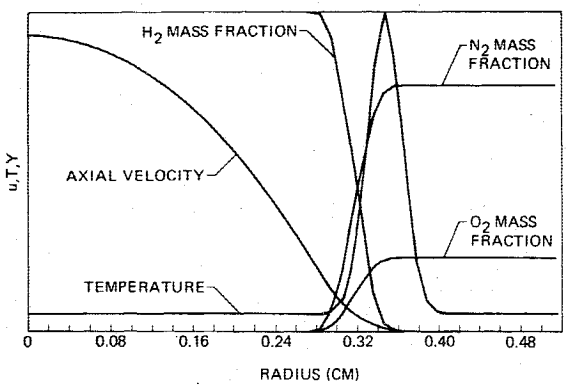

Fig. 1 Qualitative shapes of the initial condition profiles.

proceed faster than $H+O_2+M \rightarrow HO_2+M$. Otherwise the reaction will not be sustained downstream. The exact forms of the initial conditions are relatively unimportant, and the qualitative shapes are given in Fig. 1.

Numerical Method

Operator Splitting

The numerical technique that is developed here is a split-operator finite-difference method. Two operators are formulated to handle the fluid-mechanical and the chemical contributions to the solution in ways commensurate with their physical behavior. The theoretical basis for operator splitting (also called the method of fractional steps) was documented carefully in 1971 by Yanenko.[8] Probably the most widely used form of operator splitting is the familiar ADI algorithm. More recently, Rizzi and Bailey[9] have developed a method to compute inviscid, reacting flows wherein the chemical rate terms and the convective terms in two spatial dimensions are split. Another splitting scheme has been used by Thomas and Wilson[10] to calculate the flow in a chemically reacting turbulent jet.

There are generally two classes of fractional-step methods. Schemes such as ADI employ a formulation whereby one or more terms are evaluated implicitly and all of the others are evaluated explicitly for a fraction of the step; then, in the next fractional step, another set of terms is taken implicitly, and an explicit combination of the remaining terms is used. The step is divided into as many fractions as there are terms to be differenced implicitly. This type of splitting is said to have absolute consistency, since each term of the differential equation is in some way represented during each fractional step. The other class of methods allows one or more terms during each fractional step to be considered alone while the remaining terms are ignored. These methods, called majorant splitting, probably are more appropriate for chemically reacting flow problems. The equations that result from the terms being considered can be solved by numerical methods that are well suited to the behavior of each equation. This method, however, produces consistency only after all fractional steps are completed and not during each fractional step. Later in the present formulation, we shall see that the radial independence of the chemistry operator makes a majorant splitting method attractive.

A number of advantages accrue from operator splitting. One is the numerical stability gained by being able to use implicit difference operators efficiently. Generally, implicit marching methods are more stable than explicit ones. However, fully implicit methods normally require the solution of large linear systems of equations, a procedure that is computationally costly. It therefore becomes attractive to split the various terms and solve smaller sets of implicit equations. If the time scales of the terms in a set of equations vary widely, then it is costly to evaluate the differences involved in the slowly changing terms with the same frequency as is required for the rapidly changing ones. With operator splitting, one large step can be used to advance the slowly varying terms, whereas several smaller steps can be taken on the faster terms. Such is often the case when chemical changes occur much faster than fluid-mechanical changes.

We split the general transport equation, Eq. (9), into two parts that group the fluid-mechanics and chemical kinetics terms:

$$\rho u\xi \frac{\partial f}{\partial \xi} = -\left(\frac{V}{\eta}+B\right)\frac{\partial f}{\partial \eta} + \frac{1}{a\xi\eta}\frac{\partial}{\partial \eta}\left(\epsilon\eta\frac{\partial f}{\partial \eta}\right)+\xi d \tag{21}$$

$$\rho u\xi \frac{\partial f}{\partial \xi} = \xi S \tag{22}$$

Recall that f is a vector of $K+2$ variables, and note that both of the preceding equations are very nonlinear. The system of Eq. (22) is also stiff.

Transport Step

Consider first the fluid-mechanical step, Eq. (21). Two reasons have led us to approximate it with an implicit finite-difference operator. The parabolic nature of the equation means that the solution at any axial location should be continuously dependent on the boundary conditions at that location. If this behavior is to be represented properly, the numerical method must insure that the solution at each radial grid point will be influenced by the current boundary conditions; and only an implicit method, which couples the points, can achieve this result. The other factor that argues for an implicit procedure is the need for numerical stability when one is linearizing a set of nonlinear equations. For one step from ξ to $\xi+\Delta\xi$, the implicit difference equation, which involves three radial locations (index j) and two axial locations (index i), is written as

$$\rho_j u_j \xi \frac{f'_{i+1,j}-f_{i,j}}{\Delta\xi} = -\left(\frac{V_j}{\eta_j}+B_j\right)\frac{f'_{i+1,j+1}-f'_{i+1,j-1}}{2\Delta\eta}$$
$$+\frac{1}{a_j\xi\Delta\eta^2}\left(\frac{\epsilon_{j+1/2}\eta_{j+1/2}}{\eta_j}f'_{i+1,j+1}\right.$$
$$-\frac{\epsilon_{j+1/2}\eta_{j+1/2}+\epsilon_{j-1/2}\eta_{j-1/2}}{\eta_j}f'_{i+1,j}$$
$$\left.+\frac{\epsilon_{j-1/2}\eta_{j-1/2}}{\eta_j}f'_{i+1,j-1}\right)+d_j\xi \tag{23}$$

For each of the $K+2$ components of f, Eq. (23) represents a tridiagonal system of equations, the solution of which yields a new vector $f'_{i+1,j}$. Primed variables should not be thought of as representing any solution to the differential equations; they are simply intermediate variables in the splitting scheme. The $i+1$ index on the primed variables does not imply that those variables are correct at the ξ_{i+1} location. We retain the index, however, because, in the absence of any source terms [Eq. (22)], the primed quantities would be solutions at ξ_{i+1}; and, in any case, the actual mechanics of solving Eq. (23) are carried out as though the primed quantities do have spatial meaning.

In view of the size of the system of equations [$J(K+2)$ unknowns], Eq. (23) is solved sequentially for each of the $K+2$ components of $f'_{i+1,j}$. The solutions for any f' and all j are accomplished implicitly with a tridiagonal matrix algorithm. Since the nonlinear terms (u, V, a, B, ϵ, ρ, and d) are all functions of f, some consideration has to be given to how the terms are to be evaluated. We have used two approaches.

Our initial approach was to solve the sequence repetitively and to update the nonlinear terms continuously by evaluating them at the current iterate of $f'_{i+1,j}$. The iteration continues until each of the difference equations is satisfied to within a

specified tolerance. Although this approach works, it does not yield any direct measure of the solution accuracy. Instead, it can be said only that the solution is accurate to order $\Delta\xi$, and the value of the step size must be reduced until the solution is sufficiently correct. We later found it desirable to specify a relative local error tolerance E beforehand and to automate the step-size control to achieve that error.

The method used for error control is to take two steps of $\Delta\xi/2$ and one step of $\Delta\xi$, and then to compare the solutions at $\xi+\Delta\xi$. From this comparison, a local error e_f is defined for each component of f as

$$e_f = \max_j \left[\frac{|f'^{(1)}_{i+1,j} - f'^{(2)}_{i+1,j}|}{\max_j f'^{(2)}_{i+1,j}} \right] \tag{24}$$

where the superscript refers to the number of steps. The overall local error e is taken as the maximum of e_f for all f. Whether the step size is increased or decreased depends on whether e is greater or less than E. When the convergence has been reached ($e<E$) for some $\Delta\xi$, the solution at $\xi+\Delta\xi$ is taken as $f'^{(2)}_{i+1,j}$.

There is little precedent for imposing such a stringent error control on the solution of partial differential equations, although similar convergence tests are applied routinely in the solution of ordinary differential equations. We are requiring that $J(K+4)$ components of the solution vector converge simultaneously to the requested tolerance ($E=0.05$ in the present work).

In this one-step, two-step algorithm, the nonlinear terms are linearized and evaluated explicitly. More specifically, both $f'^{(1)}_{i+1,j}$ and $f'_{i+1/2,j}$ are based on nonlinear terms evaluated at $f_{i,j}$ and ξ. However, the second half-step $f'^{(2)}_{i+1,j}$ is based on nonlinear terms evaluated at $f'_{i+1/2,j}$ and $\xi+\Delta\xi/2$. In principle, the convergence rate of the scheme could be increased if Eq. (23) were averaged in the Crank-Nicholson manner, since the local truncation error would be decreased. However, because of the nonlinearities, we have chosen to retain the fully implicit differencing to enhance the numerical stability.

All of the nonlinear factors, except V, are found from algebraic expressions and are evaluated simply from $f'_{i,j}$. On the other hand, the continuity equation, whose solution provides the values of $V_{i,j}$, is an initial-value problem. Typical boundary-layer codes (cf. Ref. 11) solve the finite-difference analog to Eq. (4) directly. We believe here, however, that a solution to Eq. (11) is more appropriate; there are two reasons for the choice. The first is that, once values of u, T, and Y_k have been predicted at some ξ, there is a unique solution for V which is consistent with these values, and solving Eq. (4) requires more than the minimum information to determine that unique solution. Moreover, at the initial conditions, where u, T, and Y_k are specified as a function of radius alone, there is insufficient information to evaluate the ξ derivatives. We feel that the continuity equation should be evaluated in the same manner at each ξ_i as it is for the initial conditions. The second reason for choosing Eq. (11) concerns the inexactness of the initial conditions. Specifying the initial conditions essentially requires that one assume the true solution at the initial-condition plane. In general, there is no way to infer the exact physical solution; so it is important that the solution "forget" the initial conditions as rapidly as possible. Solving the continuity equation in a form in which the streamwise derivatives have been eliminated helps accomplish this goal, since the procedure does not incorporate explicitly any information from previous steps.

Inasmuch as V appears only within the transport portion of the split [Eq. (21)], it is appropriate that the terms in Eq. (11) which involve the chemical production $\dot{\omega}_k$ should be dropped, even though their inclusion causes no difficulty. Doing this is equivalent to performing the split first and then reformulating the mathematical problem associated with the transport step.

The solution technique that is applied to Eq. (11) takes advantage of the fact that the equation is linear in V. The essential features of the equation are more apparent if it is written as

$$\frac{dV}{d\eta} + P(\eta)V = Q(\eta) \tag{25}$$

where

$$P(\eta) = -\frac{1}{u}\frac{\partial u}{\partial \eta} + \frac{1}{T}\frac{\partial T}{\partial \eta} + \frac{\rho RT}{P}\sum_{k=1}^{K}\frac{1}{W_k}\frac{\partial Y_k}{\partial \eta} \tag{26}$$

and $Q(\eta)$ is the right-hand side of Eq. (11).

The $P(\eta)$ and $Q(\eta)$ functions are determined by finite-difference approximations of the η derivatives. Most of these derivatives already have been evaluated for the solution of the transport Eq. (26). By means of an integrating factor, we can integrate Eq. (25) as

$$V(\eta) = \exp\left[-\int P(\eta)\,d\eta\right]\int \exp\left[\int P(\eta)\,d\eta\right]Q(\eta)\,d\eta + C\exp\left[-\int P(\eta)\,d\eta\right] \tag{27}$$

The constant of integration C is zero, since $V(0)=0$ as a result of a symmetry condition at the jet centerline. The function $P(\eta)$ is an exact differential in η, and so the integrating factor always can be written as

$$\exp\left[-\int P(\eta)\,d\eta\right] = \frac{T}{u}\sum_{k=1}^{K}\frac{Y_k}{W_k} \tag{28}$$

The function $Q(\eta)$, on the other hand, can be evaluated only through a finite-difference approximation at each node. The integral then is evaluated by a numerical quadrature method, which fits a series of overlapping polynomials to the integral at each node. The quadrature algorithm itself introduces very little error into the solution procedure. In practice, however, accuracy degradation can develop as both u and its derivatives approach zero at the outer edge of the jet unless the terms in $Q(\eta)$ are evaluated accurately. These difficulties typically are apparent only near the initial conditions and do not seem to be a problem as the solution proceeds downstream.

Chemistry Step

Having the converged solution for the first part of the split, we now may turn our attention to the chemical production terms, Eq. (22). The solution $f'_{i+1,j}$ is thought of as predicted intermediate values of the solution, and these are used as initial conditions of Eq. (22) as it is solved to complete the step to ξ_{i+1}. Since S contains no spatial derivatives and since the momentum equation contains no chemical source term, the set of equations is a system of $K+1$ ordinary differential equations at each node j.

The system of equations is usually stiff, and its solution frequently has rapid transients. If the full set of equations were differenced and solved in the form of Eq. (11), then the step size $\Delta\xi$ would be restricted to a value that would capture the fastest transients at any radial position η. In the vicinity of the flame, the reactions are quite fast compared with the fluid-mechanical scales, and the step size would have to be quite small. In other portions of the jet, however, the source terms could be relatively small, and the step size should be controlled by fluid-mechanics considerations. The stiffness of the set of equations requires that implicit integration formulas be used to overcome the inherent step-size limitations, even in regions where the solution does not have rapid transients. Therefore, if the operators were not split, the implicit nature of the integration would require a set of J times $K+1$ equations to be solved, an extensive procedure compared with solving J sets of $K+1$ stiff equations with operator splitting.

It also should be noted that only the majorant-type split accomplishes the radial decoupling, whereas an ADI-type split still leaves the equations coupled, although explicitly.

After testing several solution methods for stiff differential equations, we found that the Hindmarsh-Gear package[1] was the most efficient. Euler backward differentiation algorithms developed instabilities as the step sizes became large. Collocation methods too became unstable if too few collocation points were used or if the local error tolerances were too loose. When other methods did converge to valid solutions, the computation times generally were longer than those required by the Gear code.

To proceed from ξ_i to ξ_{i+1} at some j, the Gear package takes as many steps as necessary to maintain the desired accuracy, and it varies the step size and order of integration dynamically to optimize computational efficiency. (A relative error tolerance of 10^{-4} has been used in the present work.) By using higher-order formulas when they are appropriate, Gear is able to take much larger steps than would be possible with the strictly lower-order routines. Also, Gear does not necessarily evaluate the Jacobian matrix at any step for which a previous estimate of the matrix is sufficiently valid, and, by thus judiciously evaluating the Jacobian, it gains substantial efficiency over more straightforward integration methods. In all cases, we have used finite-difference Jacobian evaluations rather than analytic evaluations. The result of the integration of Eq. (22) from the initial conditions found by solving Eq. (21) now represents a valid solution to the full equations.

Symmetric Operator

It has been shown by previous investigators[9-12] that a split symmetric operator often can lead to improved accuracy and efficiency of a numerical method. Although the improvement can be proved for certain operators, this is not the case in the present work, where the chemistry operator is a multistep variable-order algorithm. Even so, it is reasonable to expect that some advantage will be gained by using a symmetric operator. Moreover, we realize a computational savings from the symmetric operator in addition to any potential gain in convergence rate.

Let us consider two operators which, when applied twice, advance the solution from ξ_i to ξ_{i+2}. We represent this procedure with a transport and a chemistry operator in the following expression:

$$f_{i+2,j} = L_T L_c L_c L_T f_{i,j} \tag{29}$$

The first L_T operator provides a predicted value of $f'_{i+1,j}$; then the first L_c operator does a correction of that first step. Then, since the sequence does not repeat with another $L_T L_c$ operation, the chemistry operator continues on to $i+2$, the L_c now forming the predictor and L_T the corrector.

It is preferable to restart the stiff ordinary differential equation integrator code as infrequently as possible, since there is some overhead associated with the startup algorithms. Specifically, the integrator begins with low-order methods and uses a small step size to obtain the required accuracy. Then, as the integration progresses, the history of the solution can be used to form higher-order difference approximations and so allow larger step sizes. Thus, proceeding from ξ_i to ξ_{i+2} without interrupting the integrator permits a more efficient utilization of the variable step size and order features of the ordinary differential equation solver. The result of the second chemistry operator is a predicted solution at ξ_{i+2}, which the transport operator then uses as initial conditions to complete the step.

Grid System

The appropriate step size $\Delta\xi$ is chosen by the first transport operator to maintain a specified error. The chemistry operator then typically takes many steps to advance the solution to predicted values at $\xi+2\Delta\xi$. The transport operator, now called to compute a corrector step from $\xi+\Delta\xi$ to $\xi+2\Delta\xi$, may have to take smaller steps (of less than $\Delta\xi$) in order to maintain the desired accuracy. Thus the step size really should be thought of as the distance over which the operator split occurs, since, for the actual integration, all of the operators except the first L_T may use other step sizes.

At the end of one full symmetric step, the coordinate system is examined and modified as necessary. Even though only the value of f at the outer edge is specified as a boundary condition, we must maintain the condition that $\partial f/\partial\eta$ be nearly zero. However, since the derivative approaches zero only as η approaches infinity, one must be satisfied with guaranteeing that $\partial f/\partial\eta$ does not grow beyond some upper-bound δ_u. On the other hand, $\partial f/\partial\eta$ should be specified to be larger than some lower-bound δ_L; otherwise resolution is lost near the flame when too many nodes are being placed in the asymptotic region of the solution. Therefore, if $\partial f/\partial\eta$ and $\eta=\eta_e$ is outside the bounds $\delta_L < \partial f/\partial\eta < \delta_u$, the coordinate system is changed for the next step. The spread angle α is either increased or decreased by an increment $\Delta\alpha$. The same grid points are used at ξ_i, so that no interpolation is required when the coordinate system changes. It is clear that, when α changes, then ξ_0 also must change for the next step. (The redefinition of these terms is depicted in Fig. 2.) The result of the regridding procedure is that the coordinate system dynamically changes as necessary to conserve energy, momentum, and species and yet retains a maximum number of nodes in the region of interest.

Discussion of the Method

A typical flame calculation is used here as the basis for discussing the results of the numerical method. Consider a hydrogen jet with a 0.635-cm diameter and a maximum velocity of 1000 cm/s which is issuing into still, 300 K air at 1 atm. The calculated isotherm plot, together with the grid system that is generated during the computation, is shown in Fig. 3. Peak temperatures are slightly above 2000 K, and the flame length is about 4 cm.

Grid Network

The flame exhibits a very rapid radial growth in a high-gradient region just as the jet exits the nozzle. The grid generation algorithm in the code produces the required fine axial grid spacing in this region. As the flame spreads, the coordinate system does also, producing a coarser radial spacing. However, as the solution proceeds downstream, the gradients become less steep, and the coarser grid still retains the needed resolution.

In the present calculation, we use a total of 50 equally spaced radial nodes, which is adequate to resolve the steepest gradients for any of the species. Unlike boundary-layer flows in which nodes should be concentrated near the wall, the diffusion flame has no such unique region in which high resolution is required. Generally, the gradients for the minor

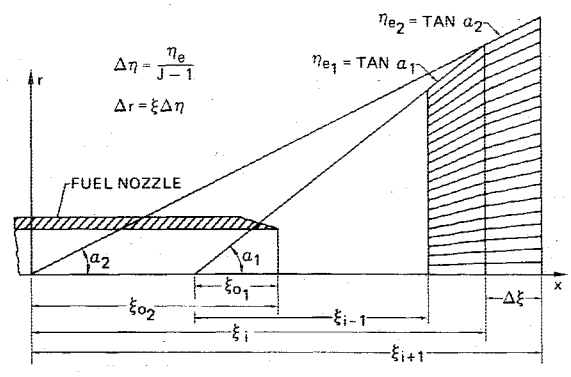

Fig. 2 Coordinate system drawn in the physical coordinates, showing a change in spread angle between steps.

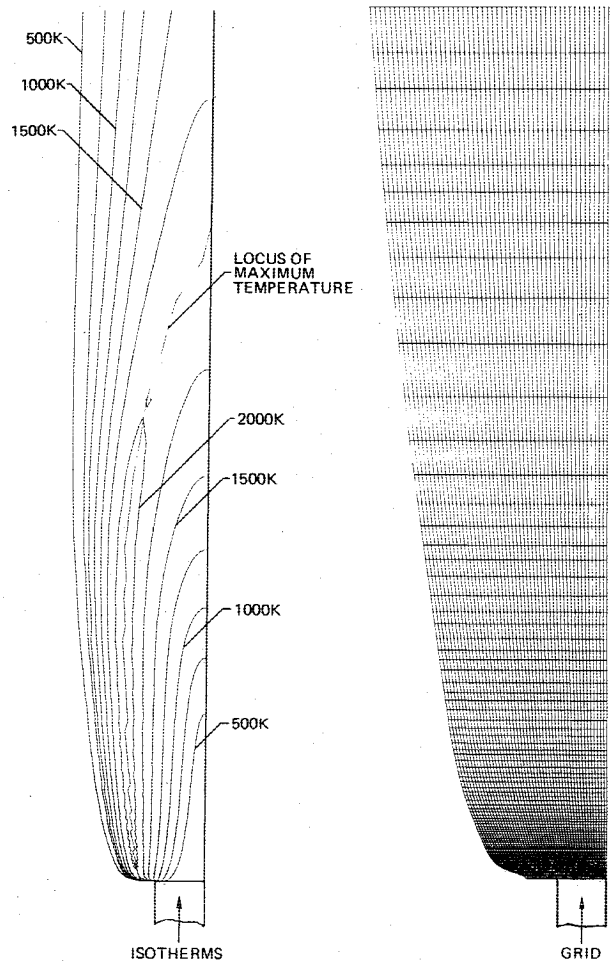

Fig. 3 Isotherms and grid system for 1000-cm/s maximum velocity H-air diffusion flame.

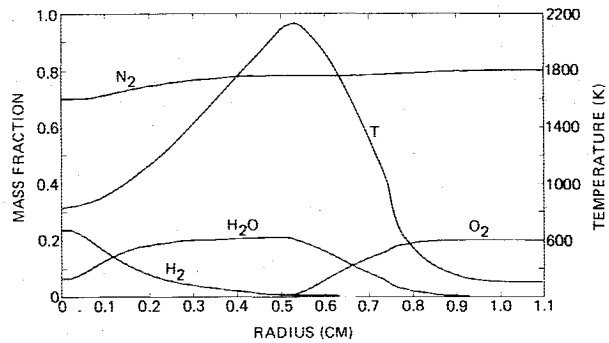

Fig. 4 Major species and temperature profiles at 1.5 cm from nozzle exit.

species such as free radicals are much sharper than those for the major species or the temperature or velocity. Compare, for example, the various radial profiles at 1.5 cm from the nozzle exit. Figures 4 and 5 reveal rather smooth profiles for the major species, temperature, and velocity. On the other hand, a profile of the OH radical in Fig. 6 is much more peaked. Also plotted in Fig. 6 are the chemical equilibrium values of OH (which reveal that the flame is well out of equilibrium). Even sharper than the minor species, in some cases, are the profiles of the local heat release from the various elementary reactions (Fig. 7). Consequently, to determine the adequate number of radial nodes, it is necessary that we look at more than the overall flame characteristics.

Although the minor species control the grid spacing, we find that the radial grid growth typically is governed by the thermal gradients, which extend further into the ambient air

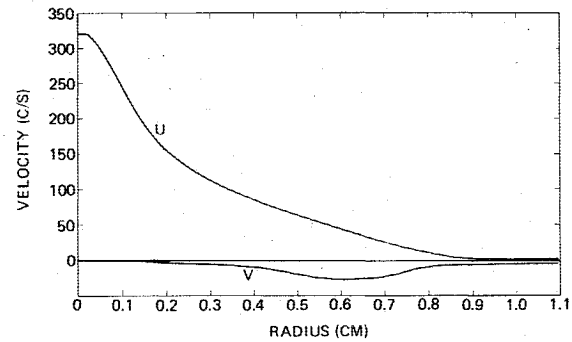

Fig. 5 Axial and radial velocity profiles at 1.5 cm from nozzle exit.

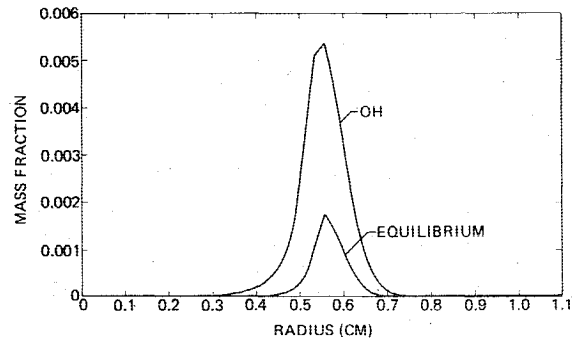

Fig. 6 Mass fraction of OH and equilibrium mass fraction of OH at 1.5 cm from nozzle exit.

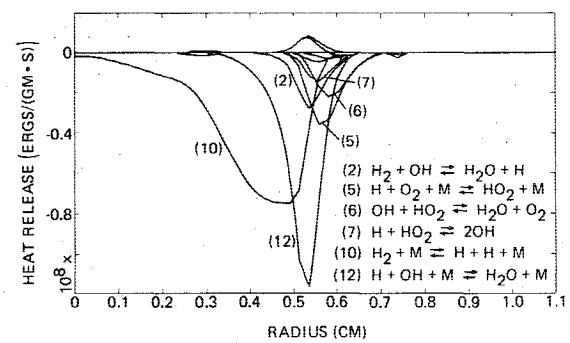

Fig. 7 Radial profiles of the contribution of the elementary reactions to heat release.

than do either the shear or species gradients. This result is not unexpected, since the reaction mechanism is highly temperature-dependent and since the peak temperatures occur well outside the regions of maximum velocity.

The axial step size begins quite small near the nozzle exit and then grows until, at the end of the problem, it is about equal to one nozzle radius. For this problem, a total of about 200 axial steps is required, with fine spacing near the nozzle, principally to accommodate a need for high resolution because the flame grows so rapidly. Although this is a region of rapid axial as well as radial change, it should be noted that in the transformed coordinates the axial change is not as rapid as it is in the physical coordinates because the grid system tends to align itself with the flame growth.

Splitting

When using a symmetric split-operator approach, one has to decide whether to consider the solutions after an $L_T L_c L_c L_T$ sequence or after an $L_c L_T L_T L_c$ sequence. Both yield valid solutions to the difference equations, and yet the resulting numbers do vary. In fact, only for a vanishingly small step size will the numbers be identical. For example, if the sequence is ended with an L_T, the combustion product species

in the flame zone are less plentiful than if the sequence is ended with an L_c operator, since these species will have partially diffused away. In practice, this effect is most apparent near the nozzle. In that region we observe that, for similar points in the flame, say around the peak temperature, the solutions after an L_c step are changing slowly as the integration proceeds downstream. The solutions after the L_T step, on the other hand, are converging toward the solutions that are obtained after the L_c step. Since we expect the structure of the narrow flame zone to be relatively insensitive to the downstream position, and since the solution after an L_T step is converging to that after an L_c step, we choose to consider the solution valid after each $L_cL_TL_TL_c$ sequence. Presumably, the inaccuracy after an L_T step can be caused by initial conditions in which the gradients are too steep, thus indicating that diffusion of species and energy is occurring at rates faster than physical until the solution has adjusted from these initial conditions.

Although it apparently is not needed for the flames presently being studied, one can envision situations in which an additional constraint on the step size is required. In the present method, the step size is chosen in order to force convergence of the transport operator in one step. If, however, this step size becomes so large that the solutions after an L_T or an L_c step are not within a certain tolerance of each other, then it would be desirable to decrease the step size further.

Computer Time

Computer time for the problem discussed here is 4 h on a CDC 6600. That time, of course, depends on the error tolerances specified and on the number of radial nodes used. Since the transport method is first-order in the marching direction, the computer time is strongly dependent on the error tolerance there. In principle, the convergence rate on the transport operator could be increased by a Crank-Nicholson averaging, but the nonlinearities in the equations somewhat cloud that certainty. In any case, although the decreased truncation error would not increase the accuracy, it should decrease the running time.

The chemistry operator employs a variable-order algorithm that internally selects the order to minimize computer time and yet still maintains the requested accuracy. Consequently, since high-order methods are available, the computation is still quite efficient when more accuracy is requested. Even so, the bulk of the overall computing time is spent doing the chemistry step.

The present computation is clearly an expensive one and most of the time is taken near the nozzle, where very rapid transients occur. Because changes are occurring so rapidly in the flowfield, very small step sizes have to be used in order to maintain the desired accuracy. Also, in this region the chemical ignition process is occurring which results in a difficult chemical kinetic computation. Since the velocities are low in the flame zone, the chemical kinetics problem is analogous to integration over a very long time step even though the axial step is small.

Conclusions

We have demonstrated an effective tool for studying the detailed structure of jet diffusion flames. Such a code allows the careful evaluation of convection, diffusion, and chemical production for any species at any point in the flame. In fact, a companion paper[2] is devoted to discussing these fluid-mechanics and combustion aspects of the hydrogen diffusion flame.

Acknowledgment

This work was supported by the U.S. Energy Research and Development Administration under Contract No. AT-(29-1)-7891.

References

[1] Hindmarsh, A. C., "Linear Multistep Methods for Ordinary Differential Equations: Method Formulations, Stability, and the Methods of Nordsieck and Gear," Lawrence Livermore Lab., UCRL-51186, March 20, 1972.

[2] Miller, J. A. and Kee, R. J., "Chemical Non-Equilibrium Effects in Hydrogen-Air Laminar Jet Diffusion Flames," *Spring Meeting*, Central States Sec., the Combustion Inst., March 28-30, 1977; also *Journal of Physical Chemistry* (to be published).

[3] Krause, E., "On the Numerical Solution of the Boundary Layer Equations," New York Univ., Rept. NYU-AA-66-57, June 1966.

[4] Svehla, R. A., "Estimated Viscosities and Thermal Conductivities of Gas at High Temperature," NASA TR R-132, 1962.

[5] Pohl, J. H., "Kinetics of Nitric Oxide and Carbon Monoxide in Combustion Systems," M.S. Thesis, Massachusetts Inst. of Technology, 1972.

[6] Gordon, S. and McBride, B. J., "Computer Program for Calculation of Complex Chemical Equilibrium Compositions, Rocket Performance, Indident and Reflected Shocks, and Chapman-Jouguet Detonations," NASA SP-273, 1971.

[7] Schlichting, H., *Boundary Layer Theory*, 6th ed., McGraw-Hill, New York, 1968, p. 220.

[8] Yanenko, N. N., *The Method of Fractional Steps*, Springer-Verlag, New York, 1971.

[9] Rizzi, A. W. and Bailey, H. E., "A Generalized Hyperbolic Marching Method for Chemically Reacting Three-Dimensional Supersonic Flow Using a Splitting Technique," *Proceedings, AIAA Second Computational Fluid Dynamics Conference*, Hartford, Conn., June 1975, pp. 38-46.

[10] Thomas, P. D. and Wilson, K. H., "Efficient Computation of 'Stiff' Chemically Reacting Flow in Turbulent Free Jets," *Proceedings, AIAA Second Computational Fluid Dynamics Conference*, Hartford, Conn., June 1975, pp. 124-132.

[11] Blottner, F. G., "Finite Difference Methods of Solution of the Boundary Layer Equations," *AIAA Journal*, Vol. 8, Feb. 1970, pp. 193-205.

[12] Strang, G., "On the Construction and Comparison of Difference Schemes," *SIAM Journal of Numerical Analysis*, Sept. 1968, pp. 506-517.